Electronic properties of strongly correlated states in dicyanoquinonediimine-Cu organic conductors

T. Ogawa and Y. Suzumura
Department of Physics, Nagoya University, Nagoya 464-01, Japan
(Received 12 June 1995; revised manuscript received 6 October 1995)

Electronic states in organic conductors, dicyanoquinonediimine-Cu (DCNQI-Cu) salts, which undergo the metal-insulator (MI) transition, have been studied based on the periodic Anderson model with electron-phonon interaction. The dimensional effects on both the metallic and insulating states are examined by taking account of the transverse hopping for the previous one-dimensional model [Phys. Rev. B **51**, 10 293 (1995)]. Within slave-boson mean-field theory, we obtain the characteristics of the strong correlation for energy bands, electronic density of states, the MI phase diagram, the specific heat, and the magnetic susceptibility. Further the MI transition in the presence of a homogeneous magnetic field is examined and compared with the transition into the antiferromagnetic state at low temperatures.

I. INTRODUCTION

Organic conductor dicyanoquinonediimine (DCNQI)-Cu salts undergo an exotic metal-insulator (MI) transition at low temperatures.[1,2] The structure of these salts shows an array of one-dimensional (1D) chains which consist of a π electron in the DCNQI molecule, and a localized d electron in the Cu atom. The hybridization between the π electron and the d electron is important in DCNQI-Cu salts since the Cu atom shows a mixed valence given by $Cu^{+4/3}$ on average.[2]

Characteristics associated with the MI transition have been found in several experiments under effective pressures, e.g., helium gas pressure,[3] and various types of $(R_1,\ R_2\text{-DCNQI})_2Cu$ with $R_1,\ R_2=$Me, MeO, Cl, and Br (Ref. 4) and deutrization.[5–8] The phase transition is of first order with a large hysteresis, which originates in the Peierls transition with a threefold lattice distortion along the chain (the c axis). The insulating state also exhibits a threefold periodicity of the valence expressed as Cu^{+}, Cu^{+}, and Cu^{2+} along the c axis. The evidence of Cu^{2+}, i.e., the local spin, has been found from the facts that the temperature dependence of the magnetic susceptibility shows the Curie law,[9] and that the MI transition is also induced by the homogeneous magnetic field.[10,11] Further, the transition from the insulating phase with local spin to the antiferromagnetic state has been found at lower temperatures below the MI transition temperature.[12,13]

The existence of a 1D band in these materials is crucial to the MI transition, since the nesting condition gives rise to the Peierls transition. However, certain facts indicate the importance of the role of the dimensional effect. The ratio of the conductivity of the c axis to that of the ab plane is about 10.[14] The coexistence of a three-dimensional (3D) Fermi surface with the 1D Fermi surface has been observed by the de Haas–van Alphen method, and the corresponding band structure is calculated by use of the tight-binding approximation.[15] The electronic structures of the metallic states have been studied from the first-principles method of the local-density-functional theory.[16] It was shown that the essential features of the observed Fermi surface of DCNQI-Cu salts, including the 3D behavior, are well reproduced, and that the electron correlation and electron-phonon interaction may be of moderate strength for the explanation of the electronic specific heat and the magnetic susceptibility.

Since the local spin of Cu^{2+} indicates the large magnitude of the Coulomb interaction, the MI transition in the presence of strongly correlated states has been studied theoretically.[17–25] A 1D model has been proposed where the chain consists of a periodic Anderson model with electron-phonon interaction. The fact that the MI transition is triggered by the Peierls transition has been shown by treating the on-site repulsive interaction within the conventional Hartree-Fock approximation.[17] Further, the MI transition was examined by applying the slave-boson theory in order to treat strongly correlated states with the local spin.[21,23] The phase diagram of the metallic state and the insulating state was obtained on the plane of temperature and the electron-phonon coupling constant. The temperature dependence of the magnetic susceptibility and specific heat was calculated within the 1D model and compared with those of experiments.[24] However, it is not yet clear what effect the 3D band has on the MI transition and the electronic states.

In the present paper, the MI transition is examined by taking account of the transverse hopping for the previous 1D model.[24] In Sec. II, a formulation is given by use of the slave-boson mean-field theory. The electronic density of states is also obtained. In Sec. III, a phase diagram of metal vs insulator is examined on the plane of temperature and the electron-phonon coupling constant. We calculate the electronic density of states, the temperature dependence of the specific heat, and the magnetic susceptibility. Further, the effect of the magnetic field on the MI transition is examined. Section IV is devoted to a discussion.

II. SLAVE-BOSON MEAN-FIELD THEORY

We consider a model given by an array of 1D chains which consist of both the conduction electron in DCNQI molecules and the d electron in Cu atoms. The Hamiltonian is given by[21,24]

$$H=\sum_{i=1}^{N}\sum_{\vec{l}}^{N_\perp}\Bigg[\sum_{\sigma=\uparrow,\downarrow}\Bigg\{t\sum_{\alpha=x,y}[C^\dagger_{\alpha i\sigma}(\vec{l})C_{\alpha i+1\sigma}(\vec{l})+\mathrm{H.c.}]+\varepsilon_d d^\dagger_{i\sigma}(\vec{l})d_{i\sigma}(\vec{l})$$
$$+V\sum_{\alpha=x,y}[C^\dagger_{\alpha i\sigma}(\vec{l})d_{i\sigma}(\vec{l})+C^\dagger_{\alpha i\sigma}(\vec{l})d_{i\sigma}(\vec{l}+\vec{\delta}_\alpha)+\mathrm{H.c.}]\Bigg\}+Ud^\dagger_{i\uparrow}(\vec{l})d_{i\uparrow}(\vec{l})d^\dagger_{i\downarrow}(\vec{l})d_{i\downarrow}(\vec{l})\Bigg]$$
$$-\frac{1}{\sqrt{NN_\perp}}\sum_{i,\vec{l},\sigma}\sum_{q}e^{iqr_i}(B_q+B^\dagger_{-q})\Bigg\{-g_\pi\sum_{\alpha}C^\dagger_{\alpha i\sigma}(\vec{l})C_{\alpha i\sigma}(\vec{l})+g_d d^\dagger_{i\sigma}(\vec{l})d_{i\sigma}(\vec{l})\Bigg\}+\sum_q\omega_q B^\dagger_q B_q, \tag{1}$$

where the hole picture is used. i denotes the lattice site along the 1D chain (the z axis). The vector $\vec{l}$ denotes the square lattice point of the unit cell in the x-y plane, where two vectors $\vec{\delta}_x$ and $\vec{\delta}_y$ are those for the nearest neighbors of $\vec{l}$. In Fig. 1, the schematic structure in the x-y plane perpendicular to the chain is shown, where the open and closed circles denote the DCNQI molecule and the Cu atom, respectively. The unit cell enclosed by the dotted square corresponds to the 1D model studied previously.[24] In Eq. (1), quantities $C^\dagger_{\alpha i\sigma}(\vec{l})$ and $d^\dagger_{i\sigma}(\vec{l})$ represent the creation operators of the π electron for two kinds of DCNQI ($\alpha=x,y$) and the d electron in the Cu atom, respectively. Quantities t, ε_d, and U are the hopping energy along the z axis, the energy level of the d electron, and the magnitude of the on-site repulsive interaction, respectively. The V term, the hybridization of which is shown by the solid line between the open and closed circles in Fig. 1, gives rise to the three-dimensional effect due to the transverse hopping perpendicular to the chain. The quantity $B^\dagger_q$ denotes the creation operator of the phonon with momentum q and energy ω_q, where g_π (g_d) is the matrix element of interaction between the phonon and the π electron (d electron). The case in which $q=\pm Q=\pm 2\pi/3$ is examined due to the threefold lattice distortion in the insulating state. Quantities t and $\hbar$ and the lattice constants are taken as unity.

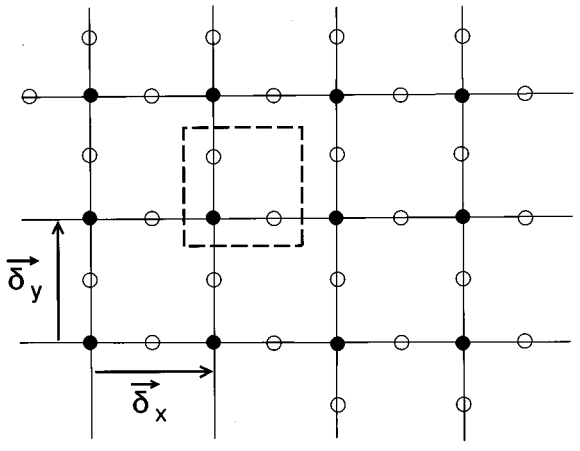

FIG. 1. Schematic structure of DCNQI-Cu salts in the plane perpendicular to the one-dimensional chain, where open and closed circles denote the DCNQI molecule and Cu atom, respectively. The domain enclosed by the dotted square is the unit cell for the 1D model (Refs. 23 and 24). The vectors $\vec{\delta}_x$ and $\vec{\delta}_y$ are unit vectors for the square lattice.

We deal with Eq. (1) as follows.

(i) In the insulating state, a threefold periodicity along the chain is assumed for the magnitude of the lattice distortion, i.e., $\langle B_{\pm Q}\rangle\neq 0$ with $Q=2\pi/3$, which is calculated self-consistently. Then the interaction between the electron and phonon in Eq. (1) induces the molecular fields acting on the π electron (d electron), which is expressed as

$$W=\frac{g_\pi}{\sqrt{NN_\perp}}\langle B_Q+B^\dagger_{-Q}\rangle, \tag{2a}$$

$$W_d=\frac{g_d}{\sqrt{NN_\perp}}\langle B_Q+B^\dagger_{-Q}\rangle=(g_d/g_\pi)W. \tag{2b}$$

The ratio of g_d to g_π is fixed by considering a phonon mode with spectrum ω_Q.[21]

(ii) The strongly correlated states originating in large U are treated in terms of the slave-boson method with the replacement of $d^\dagger_{i\vec{l}}\equiv f^\dagger_{i\vec{l}\sigma}b_{i\vec{l}}$ where $f^\dagger_{i\vec{l}\sigma}$ and $b^\dagger_{i\vec{l}}$ are creation operators for the pseudofermion and the slave boson, respectively.[26,27] By use of Lagrange's multiplier $\lambda_{i\vec{l}}$, the local constraint given by $b^\dagger_{i\vec{l}}b_{i\vec{l}}+\Sigma_{\sigma=\uparrow,\downarrow}f^\dagger_{i\vec{l}\sigma}f_{i\vec{l}\sigma}=1$ is expressed as

$$\sum_{i,\vec{l}}\lambda_{i\vec{l}}\Bigg(\sum_\sigma f^\dagger_{i\vec{l}\sigma}f_{i\vec{l}\sigma}+b^\dagger_{i\vec{l}}b_{i\vec{l}}-1\Bigg), \tag{3}$$

which is added to Eq. (1). In the present paper, mean-field theory is applied to the slave boson with threefold periodicity, i.e., $\langle b_{3n+j,\vec{l}}\rangle=\langle b_j\rangle$ and $\lambda_{3n+j,\vec{l}}=\lambda_j$, where $j=1$, 2, and 3 and n is an integer. The quantity $\langle b_j\rangle$ can be taken as real. Note that the valence X of Cu^{+X} is expressed in terms of $\langle b_j\rangle$ as

$$X=2-\tfrac{1}{3}\sum_{j=1}^{3}\langle b_j\rangle^2. \tag{4}$$

Since DCNQI-Cu salts correspond to the case of $X\simeq 4/3$, parameters are chosen so as to satisfy $\Sigma_j\langle b_j\rangle^2/3\simeq\frac{2}{3}$ for the metallic state at zero temperature.

(iii) The V term is diagonalized by rewriting operators as

$$C_{i\vec{p}\sigma}=\frac{1}{K_0(\vec{p})}\{C_{xi\vec{p}\sigma}(1+e^{-i\vec{p}\cdot\vec{\delta}_x})+C_{yi\vec{p}\sigma}(1+e^{-i\vec{p}\cdot\vec{\delta}_y})\}, \tag{5a}$$

$$\bar{C}_{i\vec{p}\sigma}=\frac{1}{K_0(\vec{p})}\{C_{xi\vec{p}\sigma}(1+e^{i\vec{p}\cdot\vec{\delta}_y})-C_{yi\vec{p}\sigma}(1+e^{i\vec{p}\cdot\vec{\delta}_x})\}, \tag{5b}$$

where Eqs. (5a) and (5b) correspond to bonding state and antibonding states of the π electron, respectively, and $K_0(\vec{p})$ is given by

$$K_0(\vec{p})=2\left[\left(\cos\frac{\vec{p}\cdot\vec{\delta}_x}{2}\right)^2+\left(\cos\frac{\vec{p}\cdot\vec{\delta}_y}{2}\right)^2\right]^{1/2}. \tag{6}$$

In Eqs. (5a) and (5b), $C_{\alpha i\vec{p}\sigma}$ with $\alpha=x$ and y are the Fourier transform for the momentum $\vec{p}$ in the x-y plane, and are given by

$$C_{\alpha i\vec{p}\sigma}=\frac{1}{\sqrt{N_\perp}}\sum_{\vec{l}} C_{\alpha i\sigma}(\vec{l})\exp(-i\vec{p}\cdot\vec{l}), \tag{7a}$$

$$f_{i\vec{p}\sigma}=\frac{1}{\sqrt{N_\perp}}\sum_{\vec{l}} f_{i\sigma}(\vec{l})\exp(-i\vec{p}\cdot\vec{l}). \tag{7b}$$

In addition to Eqs. (7a) and (7b), we make use of the Fourier transform for the z component, k $(3n+j=i,\ j=1,2,3)$,

$$O_{kj\vec{p}}=\left(\frac{3}{N}\right)^{1/2}\sum_{n}^{N/3} O_{3n+j,\vec{p}}\exp[-i(kr_{3n})], \tag{8}$$

which is useful for calculating the state with threefold periodicity along the chain.

Based on the above treatments of (i), (ii), and (iii), we rewrite Eq. (1) as

$$H_{\rm MF}=\sum_{|k|<Q/2}\sum_{|p_x|,|p_y|<\pi}\sum_{\sigma=\uparrow,\downarrow}[\Psi^\dagger_{k\vec{p}\sigma}\vec{\vec{H}}^{(a)}_{\rm MF}(k,\vec{p})\Psi_{k\vec{p}\sigma}+\bar{\Psi}^\dagger_{k\vec{p}\sigma}\vec{\vec{H}}^{(b)}_{\rm MF}(k,\vec{p})\bar{\Psi}_{k\vec{p}\sigma}]+\frac{NN_\perp}{3}\sum_j \lambda_j(|\langle b_j\rangle|^2-1)+NN_\perp\frac{W^2}{g}, \tag{9}$$

where $g=2g_\pi^2/\omega_Q$, and

$$\vec{\vec{H}}^{(a)}_{\rm MF}(k,\vec{p})=\begin{pmatrix} -W & 1 & e^{-i3k} & V_1(\vec{p}) & 0 & 0\\ 1 & -W & 1 & 0 & V_2(\vec{p}) & 0\\ e^{i3k} & 1 & 2W & 0 & 0 & V_3(\vec{p})\\ V_1(\vec{p}) & 0 & 0 & E_1 & 0 & 0\\ 0 & V_2(\vec{p}) & 0 & 0 & E_2 & 0\\ 0 & 0 & V_3(\vec{p}) & 0 & 0 & E_3 \end{pmatrix}, \tag{10}$$

$$\vec{\vec{H}}^{(b)}_{\rm MF}(k,\vec{p})=\begin{pmatrix} -W & 1 & e^{-i3k}\\ 1 & -W & 1\\ e^{i3k} & 1 & 2W \end{pmatrix}. \tag{11}$$

Matrices (10) and (11) are represented on the basis of $\Psi^\dagger_{k\vec{p}\sigma}=(C^\dagger_{k1\vec{p}\sigma},\ C^\dagger_{k2\vec{p}\sigma},\ C^\dagger_{k3\vec{p}\sigma},\ f^\dagger_{k1\vec{p}\sigma},\ f^\dagger_{k2\vec{p}\sigma},\ f^\dagger_{k3\vec{p}\sigma})$ and $\bar{\Psi}^\dagger_{k\vec{p}\sigma}=(\bar{C}^\dagger_{k1\vec{p}\sigma},\ \bar{C}^\dagger_{k2\vec{p}\sigma},\ \bar{C}^\dagger_{k3\vec{p}\sigma})$, respectively, where $E_j=\varepsilon_d-2W_d\cos Qr_j+\lambda_j$ and $V_j(\vec{p})=V\langle b_j\rangle K_0(\vec{p})$. The dimensional effect is determined by the term $V_j(\vec{p})$ in Eq. (10), since $\vec{p}$ is the momentum perpendicular to the 1D axis. The case of $V_j(\vec{p})=0$, which is obtained at $\vec{p}=(\pm\pi,\pm\pi)$ or $\vec{p}=(\pm\pi,\mp\pi)$, leads to the crucial effect on the electronic state. Quantities $\langle b_j\rangle$, λ_j, and W in Eq. (9) are determined self-consistently by

$$\langle b_j\rangle=-\frac{V}{\lambda_j}\frac{3}{NN_\perp}\sum_{k,\vec{p}}\sum_\sigma\langle C^\dagger_{kj\vec{p}\sigma}f_{kj\vec{p}\sigma}\rangle K_0(\vec{p}), \tag{12}$$

$$1=|\langle b_j\rangle|^2+\frac{3}{NN_\perp}\sum_{k,\vec{p}}\sum_\sigma\langle f^\dagger_{kj\vec{p}\sigma}f_{kj\vec{p}\sigma}\rangle, \tag{13}$$

$$-\frac{W}{g}=\frac{1}{NN_\perp}\sum_{k,\vec{p},\sigma}\sum_{j=1}^{3}\left(\langle C^\dagger_{kj\vec{p}\sigma}C_{kj\vec{p}\sigma}\rangle+\langle\bar{C}^\dagger_{kj\vec{p}\sigma}\bar{C}_{kj\vec{p}\sigma}\rangle-\frac{W_d}{W}\langle f^\dagger_{kj\vec{p}\sigma}f_{kj\vec{p}\sigma}\rangle\right)\cos Qr_j. \tag{14}$$

The chemical potential μ in Eqs. (12)–(14) is determined by

$$3=\frac{1}{NN_\perp}\sum_{k,\vec{p}}\sum_j\sum_\sigma(\langle C^\dagger_{kj\vec{p}\sigma}C_{kj\vec{p}\sigma}\rangle+\langle f^\dagger_{kj\vec{p}\sigma}f_{kj\vec{p}\sigma}\rangle+\langle\bar{C}^\dagger_{kj\vec{p}\sigma}\bar{C}_{kj\vec{p}\sigma}\rangle), \tag{15}$$

which denotes the fact that the total number of electrons per unit cell is three. The quantity $\langle\ \rangle$ in Eqs. (12)–(15) is calculated by use of Eq. (9) as

$$\langle(\Psi^{\dagger}_{k\vec{p}\sigma})_i(\Psi_{k'\vec{p}',\sigma'})_j\rangle=\delta_{k,k'}\delta_{\vec{p},\vec{p}'}\delta_{\sigma,\sigma'}\sum_m f(E^{(m)}_{k\vec{p}})\alpha^*_{m,i}\alpha_{m,j}, \tag{16a}$$

$$\langle(\overline{\Psi}^{\dagger}_{k\vec{p}\sigma})_i(\overline{\Psi}_{k'\vec{p}',\sigma'})_j\rangle=\delta_{k,k'}\delta_{\vec{p},\vec{p}'}\delta_{\sigma,\sigma'}\sum_m f(\bar{E}^{(m)}_{k\vec{p}})\bar{\alpha}^*_{m,i}\bar{\alpha}_{m,j}, \tag{16b}$$

where $f(x)=1/(e^{\beta(z-\mu)}+1)$, and $T(=\beta^{-1})$ is the temperature. Equations (16a) and (16b) are derived by use of the Green function given by $[\omega_n=(2n+1)\pi T]$,

$$G_\sigma(i\omega_n,k,\vec{p})=-\int_0^\beta d\tau\langle T_\tau\Psi_{k\vec{p}\sigma}(\tau)\Psi^{\dagger}_{k\vec{p}\sigma}(0)\rangle e^{i\omega_n\tau}$$

$$=\sum_m\frac{U_mU_m^{\dagger}}{i\omega_n+\mu-E^{(m)}_{k\vec{p}}}, \tag{17a}$$

$$\bar{G}_\sigma(i\omega_n,k,\vec{p})=-\int_0^\beta d\tau\langle T_\tau\overline{\Psi}_{k\vec{p}\sigma}(\tau)\overline{\Psi}^{\dagger}_{k\vec{p}\sigma}(0)\rangle e^{i\omega_n\tau}$$

$$=\sum_m\frac{\bar{U}_m\bar{U}_m^{\dagger}}{i\omega_n+\mu-\bar{E}^{(m)}_{k\vec{p}}}, \tag{17b}$$

where $\vec{H}^{(a)}_{\rm MF}(k,\vec{p})U_m(k,\vec{p})=E^{(m)}_{k\vec{p}}U_m(k,\vec{p})$ and $U_m^{+}=(\alpha^*_{m,1},\alpha^*_{m,2},\ldots,\alpha^*_{m,6})$ for Eq. (10), and $\vec{H}^{(b)}_{\rm MF}(k,\vec{p})\bar{U}_m(k,\vec{p})=\bar{E}^{(m)}_{k\vec{p}}\bar{U}_m(k,\vec{p})$ and $\bar{U}_m^{\dagger}=(\bar{\alpha}^*_{m,1},\bar{\alpha}^*_{m,2},\bar{\alpha}^*_{m,3})$ for Eq. (11). The MI transition is examined by substituting self-consistent solutions of Eqs. (12)–(14) into the Helmholtz free energy per unit cell, which is expressed as

$$F(W)=3\mu+\frac{W^2}{g}-\frac{T}{NN_\perp}\sum_{k,\vec{p},\sigma}\left(\sum_{m=1}^{6}\ln\{1+\exp[-\beta(E^{(m)}_{k\vec{p}}-\mu)]\}+\sum_{m=1}^{3}\ln\{1+\exp[-\beta(\bar{E}^{(m)}_{k\vec{p}}-\mu)]\}\right)+\tfrac{1}{3}\sum_{j=1}^{3}\lambda_j(\langle b_j\rangle^2-1). \tag{18}$$

Self-consistency equations (12)–(15) lead to the following characteristic for the MI transition. Since Eqs. (14) and (12) are conditions for the extremum of Eq. (18) with respect to W and $\langle b_j\rangle$, respectively, there are two kinds of critical temperatures corresponding to $W\neq0$ and $\langle b_j\rangle=0$. Generally speaking, the critical temperature for $W\neq0$ does not coincide with that of $\langle b_3\rangle=0$, and then one can consider the following three states:[24] (i) the metallic state in the case of $W=0$ and $\langle b_1\rangle=\langle b_2\rangle=\langle b_3\rangle\neq0$; (ii) the insulating state in the case of $W\neq0$, $\langle b_3\rangle=0$, and $\langle b_1\rangle=\langle b_2\rangle\neq0$; and (iii) another metallic state in the case of $W\neq0$, $\langle b_3\rangle\neq0$, and $\langle b_1\rangle=\langle b_2\rangle\neq0$. In the case of DCNQI-Cu salts, the first two states have been found, while the third one has never been observed. In the present model, we also obtain only the first two states by choosing large g, which leads to the absence of the third state due to the large jump of W at the Peierls transition. Such a first-order phase transition reveals three kinds of critical temperatures which depend on the rate of variation of temperature: a rapid increase (A), a quasistatic variation (B), and a rapid decrease (C). Note that the point corresponding to the transition from $\langle b_3\rangle\neq0$ into $\langle b_3\rangle=0$ coincides with point A in the present choice of numerical parameters. When $\langle b_3\rangle$ becomes zero, the hybridization is disconnected at every third lattice point, resulting in the periodic array of Cu^{+}, Cu^{+}, Cu^{2+}, ... for the Cu atom.

For studying the dimensional effect on the electronic properties, we calculate the density of states per spin and per unit cell $D(\omega)$ expressed as

$$D(\omega)=D_c(\omega)+D_d(\omega)+D_{\bar{c}}(\omega), \tag{19}$$

where $D_c(\omega)$, $D_d(\omega)$, and $D_{\bar{c}}(\omega)$ denote the components of the density of states for the bonding π electron, the d electron, and the nonbonding π electron, respectively. The notation c is used for the π electron. By taking $i\omega_n\to\omega+i0$ in Eqs. (17a) and (17b), quantities $D_c(\omega)$, $D_d(\omega)$, and $D_{\bar{c}}(\omega)$ are obtained as

$$D_c(\omega)=\tfrac{1}{3}\sum_{i=1}^{3}D_i(\omega), \tag{20a}$$

$$D_d(\omega)=\tfrac{1}{3}\sum_{i=4}^{6}D_i(\omega), \tag{20b}$$

$$D_{\bar{c}}(\omega)=\tfrac{1}{3}\sum_{i=1}^{3}\bar{D}_i(\omega), \tag{20c}$$

where

$$D_i(\omega)=-\frac{1}{\pi}\frac{3}{NN_\perp}\sum_{k,\vec{p}}\mathrm{Im}[G_\sigma(\omega-\mu+i\delta,k,\vec{p})]_{i,i}$$

$$=\frac{3}{NN_\perp}\sum_{k,\vec{p},m}\alpha^*_{m,i}\alpha_{m,i}\delta(\omega-E^{(m)}_{k\vec{p}}), \tag{21a}$$

$$\bar{D}_i(\omega)=-\frac{1}{\pi}\frac{3}{NN_\perp}\sum_{k,\vec{p}}\mathrm{Im}[\bar{G}_\sigma(\omega-\mu+i\delta,k,\vec{p})]_{i,i}$$

$$=\frac{3}{NN_\perp}\sum_{k,\vec{p},m}\bar{\alpha}^*_{m,i}\bar{\alpha}_{m,i}\delta(\omega-\bar{E}^{(m)}_{k\vec{p}}). \tag{21b}$$

Note that $\int d\omega\ D(\omega)=3$ and $\int d\omega\ D_\alpha(\omega)=1$ for $\alpha=c$, d, and $\bar{c}$, respectively. We calculate Eqs. (21a) and (21b) by use of the formula $\delta(\omega-E_{k\vec{p}})\simeq1/(\omega_1)$ for $0<|\omega-E_{k\vec{p}}|<\omega_1/2$ and zero otherwise, where $\omega_1\ll1$.

III. METAL VS INSULATOR IN STRONG CORRELATION

We examine the MI transition and the electronic states by calculating Eqs. (12)–(15) self-consistently. Parameters are chosen as $\varepsilon_d=0.85$, $V=0.4$, and $g_d/g_\pi=0.7$, which lead to $Z=4/3$ for Cu^X in the metallic state at $T=0$.[24] A MI transition similar to that in the present section is also obtained by taking $V=0.2$ and 0.3, and a corresponding value of ε_d. There is a reasonable range for the choice of parameters leading to such a transition.

By diagonalizing Eqs. (10) and (11), the energy-band spectrum is obtained in terms of the extended zone scheme which is expressed as $E(\tilde{k},\vec{p})=E_{k\vec{p}}^{(m)}$ and $\tilde{k}=k+mQ$. Although the calculations are performed by adopting the hole picture from Sec. II, the numerical results of both the energy-band spectrum and the density of states are expressed by use of the electron picture in this section for comparison with other work. The transformations are given by $E_e(\tilde{k},\vec{p})=-E(\tilde{k},\vec{p})$, $D_e(\omega)=D(-\omega)$, and $\mu_e=-\mu$.

In the case of the metallic state ($W=0$), the energy spectrum of the electron picture for the antibonding state is given by $-2\cos\tilde{k}$ leading to the flat Fermi surface, while that for the bonding state is expressed as

$$E^{(\pm)}(\tilde{k},\vec{p})=\tfrac{1}{2}[-2\cos\tilde{k}-E\pm\sqrt{(2\cos\tilde{k}-E)^2+4|V(\vec{p})|^2}]. \tag{22}$$

In Eq. (22), $V(\vec{p})=V_j(\vec{p})$ ($j=1$, 2, and 3), and + (−) denotes the upper (lower) band. The Fermi surface of the bonding state, which is obtained from $E^{(+)}(\tilde{k},\vec{p})=\mu_e$, is shown in Fig. 2(a), where $\langle b_1\rangle=\langle b_2\rangle=\langle b_3\rangle\simeq 0.82$, $E_1=E_2=E_3=E\simeq 1.40$, and $\mu=-\mu_e=0.90$. The wave vectors $(\tilde{k},p_x,p_y)$, corresponding to corners, are given by Γ (0,0,0), $X(\pi,0,0)$, $Y(\pi,\pi,0)$, $U(\pi,0,\pi)$, $Z(0,0,\pi)$, and $V(\pi,\pi,\pi)$, respectively. In Fig. 2(b), the energy-band spectrum of the electron picture, $E_e(\tilde{k},\vec{p})$, for the metallic state is shown, where the chemical potential μ_e is indicated by the arrow. The two solid curves denote bands of the bonding state, $E^{(\pm)}(\tilde{k},\vec{p})$, consisting of a π electron and a d electron, while the dashed curve shows that of the antibonding state. In the interval region between point V and point Y, the π band of the bonding state coincides with that of the antibonding state, and the d band becomes flat due to $V(\vec{p})=0$. The energy band is compared with those obtained by Miyazaki *et al.*[16] and Uji *et al.*[15] by noting that electrons of our unit cell are half of theirs. The general features of the energy band seem to agree qualitatively. However, the details of electronic states around the Fermi surface which is shown in the interval region of Y-Γ-X depend on the method which treats the interaction and correlation. In Fig. 2(c), the energy-band spectrum of the electron picture for the insulating state is shown in the case of $g=0.7$, which leads to $W=0.76$, $E_1=E_2=1.75$, $E_3=0.95$, $\langle b_1\rangle=\langle b_2\rangle=0.94$, $\langle b_3\rangle=0$, and $\mu=-\mu_e=0.95$. The gap appears at $\tilde{k}=\pi n/3$ ($n=1,2$), where $W(\neq 0)$ is induced by the Peierls transition with threefold lattice distortion. The localized level is located at the chemical potential and is half-filled due to the local constraint of Eq. (3) with $\langle b_3\rangle=0$.

In Fig. 3, the phase diagram on the plane of the coupling constant of the electron-phonon interaction g and temperature T is shown, where the solid curves and closed square are the boundaries of the MI transition in the case of the rapid

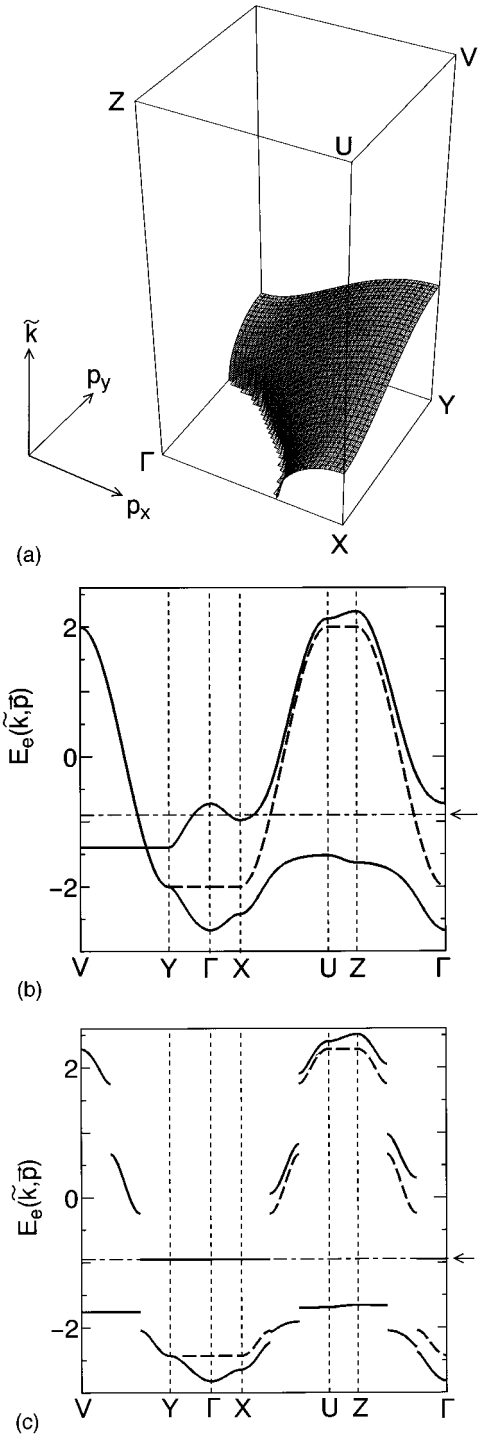

FIG. 2. (a) Fermi surface of the bonding band in the metallic state where $V=0.4$ and $W=0$. The quantity $\tilde{k}$ denotes the 1D wave number in the extended zone scheme. The wave vectors $(\tilde{k},\ p_x,\ p_y)$ for the corners are given by $\Gamma(0,0,0)$, $X(\pi,0,0)$, $Y(\pi,\pi,0)$, $U(\pi,0,\pi)$, $Z(0,0,\pi)$, and $V(\pi,\pi,\pi)$, respectively. (b) Energy-band spectrum of the electron picture for the metallic state where parameters are the same as in (a). The arrow denotes the location of the chemical potential, $\mu_e=-0.90$. (c) Energy-band spectrum of the electron picture for the insulating state with $g=0.7$ and $W=0.76$, where the arrow denotes the location of the chemical potential, $\mu_e=-0.95$.

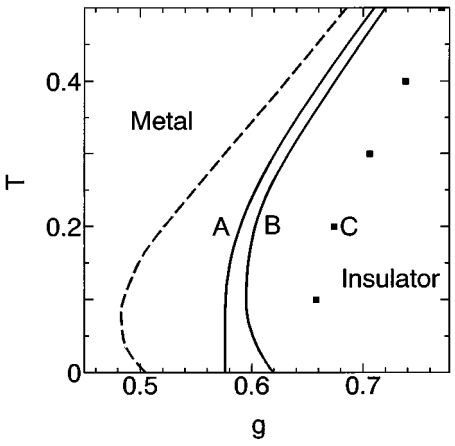

FIG. 3. Phase diagram of the metal insulator (MI) on the g-T plane where $\varepsilon_d=0.85$, $W_d/W=0.7$, and $V=0.4$. $g=g_\pi^2/\omega_Q$. The solid curves and closed square denote boundaries of the MI transition determined by the rapid increase (A), the quasistatic variation (B), and the rapid decrease (C) of temperatures. The dashed curve shows the boundary of B for the 1D model (Ref. 24).

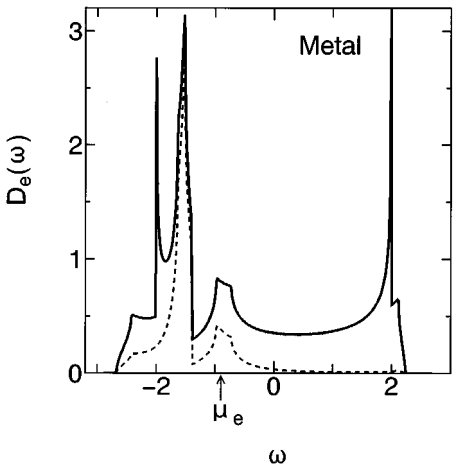

FIG. 4. Density of states of the electron picture for the metallic state corresponding to Fig. 2(b). The dotted curve denotes the component of the d electron, and μ_e is the chemical potential.

increase (A), the quasistatic variation (B), and the rapid increase (C) of temperatures. The first-order phase transition in the present case is followed by a remarkable hysteresis which comes from the large entropy of the local spin.[20] The MI boundary is steep compared with that of the conventional Hartree-Fock approximation,[22] and shows the critical value of g below which the insulating state does not exist. The existence of the critical value of g is the characteristic of the strong correlation since the energy gain by the Peierls gap competes with the vanishing of the coherent energy of the hybridization due to $\langle b_3\rangle=0$ in the insulating state. The MI boundary for the quasistatic process (curve B) is compared with that of the 1D case (dashed curve).[24] The MI boundary for the present case (3D case) is similar to that of the 1D case, where the critical value of g of the 3D case is larger than that of the 1D case. Both cases show the reentrant metal-insulator-metal (MIM) transition as a function of T. Phase transitions are classified into three groups: the metallic state down to zero temperature (group I), the metallic state into the insulating state (group II), and the reentrant transition given by MIM (group III). In Fig. 3, there is the small variation of valence X in Cu^X. The quantity X increases by the increase of T, but decreases by the increase of g. For example, we obtain that $X=1.33$, 1.37, and 1.47 for $T=0$, 0.2, and 0.4 in the metallic state, and that $X=1.45$, 1.43, and 1.41 for $g=0.6$, 0.7, and 0.8 with the fixed $T=0.2$ in the insulating state. At the $M\rightarrow I$ transition, there is a jump of X which is $\simeq+0.1$. As mentioned in Sec. II, the insulating state is always followed by $\langle b_3\rangle=0$ due to the large jump of W at the boundary of the MI transition.

By substituting the energy-band spectrum into Eqs. (21a) and (21b), we calculate the density of states of the electron picture, $D_e(\omega)$ $[=D(-\omega)]$ per spin and per unit cell at $T=0$. The quantity $D_e(\omega)$ for the metallic state is shown in Fig. 4, where the dotted curve denotes the component of the d electron. The hybridization gap which exists in the 1D case vanishes in the 3D case since $V(\vec{p})$ changes continuously and becomes zero at $\vec{p}=(\pm\pi,\pm\pi)$ or $(\pm\pi,\mp\pi)$. There are two kinds of anomalies: one is the cusp due to the 3D van Hove singularity in the bonding band, and the other is the 1D singularity in the antibonding band which is proportional to $|\omega\mp2|^{-1/2}$ at $\omega=\pm2$. The arrow denotes the chemical potential $\mu_e(=-\mu)$. The dip just below the chemical potential shows the point at which the matrix element of the hybridization, $V(\vec{p})$, vanishes. The double peaks of the density of states for the d electron is due to the effect of the hybridization. Note that the filling of the d hole above μ_e is given by $(1-\Sigma_j\langle b_j\rangle^2/3)/2$ from Eq. (3), and then becomes equal to $\frac{1}{6}$ in the metallic case. In Fig. 5, the density of states $D_e(\omega)$ for the insulating state is shown where a large gap opens due to $W\neq0$ in the Peierls state. The singularity at the chemical potential, which is expressed as $\frac{1}{3}\delta(\omega-\mu_e)$, is attributable to the localized level of the d electron in Fig. 2(c). At the energy level with $\omega=\mu_e$, the d electron is half-filled, resulting in the local spin. Such a singularity also exists in the insulating state of the 1D case. The band edge $(\omega=-1+W)$ just above the chemical potential is deter-

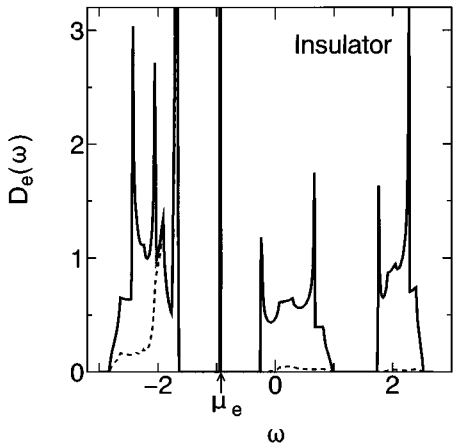

FIG. 5. Density of states of the electron picture for the insulating state corresponding to Fig. 2(c). The dotted curve denotes the component of the d electron, and μ_e is the chemical potential.

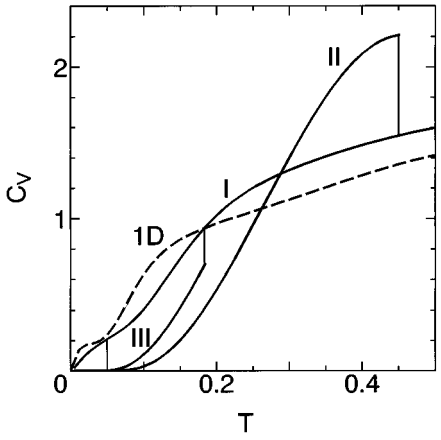

FIG. 6. The T dependence of the specific heat, C_V, in the case of $g<0.58$(I), $g=0.7$(II), and $g=0.6$(III), which show the transition of M, MI and MIM by the decrease of T, respectively. The parameters are the same as in Fig. 3. The dashed curve denotes C_V for the 1D metallic state (Ref. 24).

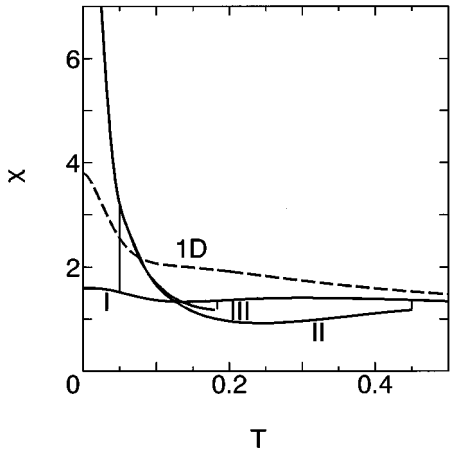

FIG. 7. The T dependence of the magnetic susceptibility (χ) in the case of $g<0.58$(I), $g=0.7$(II), and $g=0.6$(III). The dashed curve denotes χ for the 1D metallic state (Ref. 24).

mined by both the antibonding electron and the bonding electron, which leads to the divergence of $D_e(\omega)$ due to the 1D band and zero due to the 3D band, respectively. The band edge just below the chemical potential is determined only by the bonding electron. The filling of the d hole in the insulating state is slightly larger than $\frac{1}{6}$ due to $\langle b_1\rangle=\langle b_2\rangle\neq 1$.

Based on Figs. 3, 4, and 5, we study the T dependence of the specific heat and magnetic susceptibility by choosing $g=0.48$(I), 0.7(II), and 0.6 (III) which belong to parameters for groups I, II, III, respectively, in the quasistatic process. The ground state in the case of $g=0$ and 0.6 ($g=0.7$) is given by the metallic state (the insulating state), the energy band for which is shown in Fig. 2(b) [Fig. 2(c)].

The specific heat per unit cell, C_V, is obtained by substituting Eq. (18) into $C_V=-T[\partial^2 F(W)/\partial T^2]$. Figure 6 shows C_V in the case of $g=0$(I), 0.7(II), and 0.6(III) where the dashed curve denotes C_V of the metallic state for the 1D model. In the metallic state, C_V shows the T-linear dependence at low temperatures. Curve I shows that $\gamma\simeq 5.3$, where the coefficient γ is defined by $\gamma\equiv\lim_{T\to 0}C_V/T$. We also obtain $\gamma\simeq 5.3$ by use of the conventional formulas $\gamma=(2\pi^2/3)D_e(\mu_e)$ and $D_e(\mu_e)\simeq 0.80$ in Fig. 4. There is a T dependence of $D_e(\mu_e)$ which comes from both $\langle b_j\rangle$ and λ_j, e.g., $\langle b_j\rangle\simeq 0.82-0.65T^2$ and $\lambda_j\simeq 0.54-0.85T^2$ for the metallic state in Fig. 6. However, the effect of the T dependence of $D_e(\mu_e)$ on γ is negligible since a good coincidence between these two results for γ is obtained. There is the enhancement of γ due to the correlation since the case of $k_F=\pi/3$ in the absence of hybridization leads to $D_e(\mu_e)\sim 2/(\pi v_F)\simeq 0.37$ and then $\gamma\simeq 2.4$. The small reduction of C_V from the T-linear dependence at low temperatures comes from the dip of $D_e(\omega)$ in Fig. 4 which is located below the chemical potential. Such a reduction is enhanced in the 1D case due to the hybridization gap as is shown in Fig. 6. The fact that 1D γ is larger than 3D γ comes from the fact that $D_e(\mu_e)$ of the 1D case is large compared with that of the 3D case. Thus we found the visible effect of dimension for the metallic state. In the insulating state, curves II and III show the exponential decrease of C_V which originates in the Peierls gap ($W\neq 0$) around the chemical potential in Fig. 5. Actually, we obtain $C_V\propto\exp[-W_G]$, where $W_G\simeq -1+W-\mu_e$. There is a jump of specific heat at the critical temperature T_C, which is defined by $\Delta C_V[\equiv C_V(T\to T_C-0)-C_V(T\to T_C+0)]$. The fact that $\Delta C_V>0$ in curve II is similar to that of the second-order phase transition, while curve III shows $\Delta C_V<0$ at the upper T_C. Since the first-order phase transition into the insulating state is followed by both the latent heat and the entropy of the local spin, $S_l=\frac{2}{3}\ln 2$, the large reduction of C_V can be expected in the case of small T_C from the conservation law of the entropy. We note that such a fact could be useful in understanding the recent experiment on deuterized (DMe-DCNQI)$_2$Cu, which indicates $\Delta C_V<0$ at the upper T_C in the case of the reentrant transition.[28]

The static magnetic susceptibility per atom, χ, under the uniform field is calculated by taking account of the Zeeman energy

$$H_{\text{Zeeman}}=-\sum_{\sigma}\ \text{sgn}(\sigma)M_\sigma B, \tag{23}$$

where $M_\sigma=\Sigma_{i,\vec{l}}(C^\dagger_{i\vec{l}\sigma}C_{i\vec{l}\sigma}+\bar{C}^\dagger_{i\vec{l}\sigma}\bar{C}_{i\vec{l}\sigma}+f^\dagger_{i\vec{l}\sigma}f_{i\vec{l}\sigma})$. The susceptibility χ is defined by $\chi=\lim_{B\to 0}(\langle M_\uparrow\rangle_B-\langle M_\downarrow\rangle_B)/(BNN_\perp)$, where $\mu_B=1$ and $\langle\ \rangle_B$ denotes the average in the presence of the Zeeman energy. In Fig. 7, the magnetic susceptibility χ is shown for $g=0$(I), 0.7(II), and 0.6(III), where the dashed curve denotes χ of the metallic state in the 1D case. In the case of the metallic state (curve I), the T dependence of χ is similar to that of the paramagnetic susceptibility. The fact that $\chi\sim 1.6$ at $T=0$ indicates the validity of $\chi=2D_e(\mu_e)$ in the limit of zero temperature since $D_e(\mu_e)\simeq 0.80$ in Fig. 4. It is found that the enhancement of χ in the 1D case is reduced by the transverse hopping which suppresses the density of states around $\omega=\mu_e$. In the region belonging to the insulating state in curves II and III, one finds the Curie law given by $\chi\simeq 1/(6T)$ which originates in the local spin of the d electron situated on the Fermi surface. The Curie law is also obtained in the 1D model,[24] since the decoupled state of the d electron is independent of the dimension in the present approximation. The jump of χ shows a negative change at the $M\to I$ transition

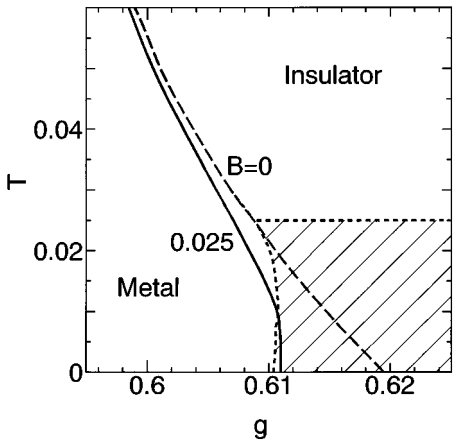

FIG. 8. Phase diagram in the presence of the homogeneous magnetic field $B(=0.025)$, where the dashed curve denotes the MI boundary for $B=0$ in Fig. 3. The hatched region belongs to the antiferromagnetic state in the presence of the AF interaction ($J=0.05$ and $B=0$).

since the effect of the formation of the Peierls gap at the Fermi surface is larger than that of the local spin. However, the enhancement of χ at the MI transition can be expected by the strict treatment of the local constraint,[27] which would result in $\chi=1/(3T)$ being twice as large as the present one.

Now we examine the MI transition in the presence of the magnetic field B by adding Eq. (23) to Eq. (9). In Fig. 8, the boundary of the MI transition in the case of $B=0.025$ is shown by the solid curve on the plane of g and T where the boundary in the case of $B=0$ is indicated by the dashed curve. The fact that the domain for the insulating state increases at low temperatures is due to the following reason. Since the energy gain by the Zeeman energy is expressed as $-\chi_I B^2$ and $-\chi_M B^2$ for the insulating and metallic states, respectively, in the case of the small B, the MI boundary is determined by the condition that $\Delta\chi B^2[\equiv(\chi_I-\chi_M)B^2>0]$ becomes equal to $\Delta F[\equiv F(W)-F(0)]$. Figure 7 shows the increase of $\Delta\chi B^2$ with the decrease of temperature, and then the domain of the insulating state is enhanced. For the small B, the B dependence of T_C is rewritten as $T_C(B)\simeq T_C(0)-KB^2$, where $K=-(g/W)^2(dT_C/dg)(\Delta\chi/2)$. Actually, the quantity K in the case of $g=0.6$ is given by $K\sim 3.7$, where $|dT_C/dg|\sim 4.7$, $\Delta\chi\sim 1.5$, and $W\sim 0.58$. We note that such a B dependence of T_C is similar to that observed in partially deuterated (DM-DCNQI)$_2$Cu salt.[11] From the MI boundary in the limit of zero temperature, it turns out that the quantity dT_C/dg is infinite (finite) for $B=0.025$ ($B=0$). Such a result comes from the fact that the entropy of the local spin reduces experimentally (remains finite) at low temperatures in the presence (absence) of magnetic field. Therefore it is expected that the interaction between localized d electrons leads to the MI boundary, similar to the solid curve, as is discussed in Sec. IV.

IV. DISCUSSION

We examined the MI transition in DCNQI-Cu salts by making use of the 3D model where the transverse hopping is taken into account between chains of the previous 1D model. The hybridization gap existing in the 1D case vanishes due to the transverse hopping, and then a remarkable effect appears in the metallic states as is found in the density of states of Fig. 4. This feature leads to the suppression of thermodynamic quantities at low temperatures, e.g., reductions of both γ and χ which are consistent with those of the experiment of (DMe-DCNQI)$_2$-Cu salts.[4] The similarity of the boundary of the MI transition in Fig. 3 to that of the 1D model comes from the property of the insulating state in which the dimensional effect is small due to the d electron being disconnected from the π electron. The existence of the critical value of g for the MI transition is a consequence of the strong correlation which leads to the competition between the energy gain of the Peierls gap and that of the hybridization gap.

In addition to the variation of g, it is significant to note the effect of ε_d on the MI transition, since pressure changes the energy of the localized level ε_d through the deformation of the tetragonal structure around the Cu atom. We obtained a MI boundary on the plane of ε_d and T which is similar to Fig. 3. In the case of $g=0.59$, the relation between ε_d and g is estimated as $\varepsilon_d\simeq 0.85-(g-0.59)/0.11$. Therefore one must take into account the variation of both g and ε_d as the effective pressure.

Finally we comment on the antiferromagnetic (AF) state which has been observed at low temperatures in the insulating state.[13] The AF state is examined by adding the interaction

$$H_{\rm spin}=J\sum_i \sum_{\langle \vec{l},\vec{l}'\rangle} S^Z_{i\vec{l}} S^Z_{i\vec{l}'}, \tag{24}$$

to the present model, Eq. (9), where $S^Z_{i\vec{l}}=(f^\dagger_{i\vec{l}\uparrow}f_{i\vec{l}\uparrow}-f^\dagger_{i\vec{l}\downarrow}f_{i\vec{l}\downarrow})/2$. In the case of DCNQI-Cu, the axis of the spin ordering Z is oriented to the direction perpendicular to the 1D axis.[4,13] By use of the mean-field approximation, Eq. (24) is rewritten as

$$H_{\rm spin}=\sum_i \left(\sum_{\vec{l}} -\Delta_i(-1)^{l_x}(-1)^{l_y}S^Z_{i\vec{l}}+N_\perp\Delta_i^2/8J \right), \tag{25}$$

where $\Delta_i\equiv 4JN_\perp^{-1}\Sigma_{\vec{l}}\langle S^Z_{i\vec{l}}\rangle(-1)^{l_x}(-1)^{l_y}$ and $\Delta_j=\Delta_{3m+j}$ ($j=1$, 2, and 3). The AF state in Eq. (25) is calculated by choosing a small J in which AF ordering occurs only for the site of the local spin. Then self-consistency equation for Δ_i is written as $\Delta_1=\Delta_2=0$ and $\Delta_3=2J\tanh(\beta\Delta_3/4)$, which is derived by treating Eq. (3) under the global constraint. The boundary for the MI transition is calculated by adding the excess energy $\delta F_{\rm spin}$ to Eq. (18), where $\delta E_{\rm spin}(\Delta_3)=-(2T/3)\ln[\cosh(\beta\Delta_3/4)]+\Delta_3^2/(24J)$. In Fig. 8, the boundaries corresponding to both the M-AF transition and the I-AF transition are shown by the dotted curve for $J=0.05$. The difference between the solid and dashed curves is small at low temperatures. This is understood from the fact that the energy per localized d electron is given by $-B$ for Eq. (23) and is given by $-\Delta^2/(8J)$ $(=-J/2)$ for Eq. (25), respectively.

It will be interesting to study the interplay of the magnetic field B and the AF interaction and the jump of χ at T_C in terms of the $1/N$ expansion which treats the local constraint strictly.[27]

ACKNOWLEDGMENTS

The authors are thankful to T. Matsuura and Y. Kuroda for useful discussion. One of the authors (T.O.) acknowledges the Fellowship of Japan Society for the Promotion of Science. This work was partially supported by a Grant-In-Aid for Scientific Research from the Ministry of Education, Science and Culture No. 05640410, and a Grant-in-Aid for Scientific Research on the priority area, Novel Electronic States in Molecular Conductors, from the Ministry of Education, Science and Culture, Japan.

[1] A. Aumüller, P. Erk, G. Klebe, S. Hünig, J. U. von Schütz, and H.-P. Werner, Angew. Chem. Int. Ed. Engl. **25**, 740 (1986).

[2] A. Kobayashi, R. Kato, H. Kobayashi, T. Mori, and H. Inokuchi, Solid State Commun. **64**, 45 (1987).

[3] S. Tomić, D. Jérome, A. Aumüller, P. Erk, S. Hünig, and J. U. von Schütz, J. Phys. C **21**, L203 (1988).

[4] H. Kobayashi, A. Miyamoto, R. Kato, F. Sakai, A. Kobayashi, Y. Yamakita, Y. Furukawa, M. Tasumi, and T. Watanabe, Phys. Rev. B **47**, 3500 (1993), and references therein.

[5] S. Hünig, K. Sinzger, M. Jopp, D. Bauer, W. Bietsch, J. U. von Schütz, and H. C. Wolf, Angew. Chem. Int. Ed. Engl. **31**, 859 (1992).

[6] K. Sinzger, S. Hünig, M. Jopp, D. Bauer, W. Bietsch, J. U. von Schütz, H. C. Wolf, R. K. Kremer, T. Metzenthin, R. Bau, S. I. Khan, A. Lindbaum, C. L. Lengauer, and E. Tillmanns, J. Am. Chem. Soc. **115**, 7696 (1993).

[7] R. Kato, H. Sawa, S. Aonuma, M. Tamura, M. Kinoshita, and H. Kobayashi, Solid State Commun. **85**, 831 (1993).

[8] S. Aonuma, H. Sawa, R. Kato, and H. Kobayashi, Chem. Lett. **1993**, 513.

[9] H. Kobayashi, R. Kato, A. Kobayashi, Y. Nishio, K. Kajita, and W. Sasaki, J. Phys. Chem. Solids **51**, 533 (1990).

[10] S. Kagoshima, A. Miyazaki, T. Osada, R. Kato, N. Miura, and H. Kobayashi, Synth. Met. **61**, 259 (1993).

[11] T. Ohgi, Ph.D. thesis, University of Tokyo, 1995; T. Ohgi, Y. Shimazu, S. Ikehata, and R. Kato (unpublished).

[12] T. Mori, H. Inokuchi, A. Kobayashi, R. Kato, and H. Kobayashi, Phys. Rev. B **38**, 5913 (1988).

[13] M. Tamura, H. Sawa, S. Aonuma, R. Kato, M. Kinoshita, and H. Kobayashi, J. Phys. Soc. Jpn. **62**, 1470 (1993).

[14] J. U. von Schütz, M. Bair, D. Bauer, W. Bietsch, M. Krebs, H. C. Wolf, S. Hünig, and K. Sinzger, Synth. Met. **55-57**, 1809 (1993).

[15] S. Uji, T. Terashima, H. Aoki, J. S. Brooks, R. Kato, H. Sawa, S. Aonuma, M. Tamura, and M. Kinoshita, Phys. Rev. B **50**, 15 597 (1994); Solid State Commun. **93**, 203 (1995).

[16] T. Miyazaki, K. Terakura, Y. Morikawa, and T. Yamasaki, Phys. Rev. Lett. **74**, 5104 (1995).

[17] Y. Suzumura and H. Fukuyama, J. Phys. Soc. Jpn. **61**, 3322 (1992).

[18] H. Fukuyama, J. Phys. Soc. Jpn. **61**, 3452 (1992).

[19] H. Fukuyama, Prog. Theor. Phys. Suppl. **113**, 125 (1993).

[20] H. Fukuyama, in *Proceedings of the 16th Taniguchi Symposium 1993, Correlation Effects in Low-Dimensional Electron Systems*, edited by A. Okiji and N. Kawakami (Springer-Verlag, Berlin, 1994), p. 128.

[21] Y. Suzumura and Y. Ōno, J. Phys. Soc. Jpn. **62**, 3244 (1993).

[22] T. Ogawa and Y. Suzumura, J. Phys. Soc. Jpn. **63**, 1494 (1994).

[23] T. Ogawa and Y. Suzumura, J. Phys. Soc. Jpn. **63**, 2066 (1994).

[24] T. Ogawa and Y. Suzumura, Phys. Rev. B **51**, 10 293 (1995).

[25] M. Nakano, M. Kato, and K. Yamada, Physica B **186-188**, 1077 (1993).

[26] P. Coleman, Phys. Rev. B **29**, 3035 (1984).

[27] B. Jin and Y. Kuroda, J. Phys. Soc. Jpn. **57**, 1687 (1988).

[28] N. Someya, Y. Nishio, K. Kajita, H. Kobayashi, S. Aonuma, H. Sawa, and R. Kato (unpublished).